Journal of Colloid and Interface Science 599 (2021) 519–532

Contents lists available at ScienceDirect

Journal of Colloid and Interface Science

journal homepage: www.elsevier.com/locate/jcis

Regular Article

Gel-like carbon dots: A high-performance future photocatalyst

Yiqun Zhou [a,1], Ahmed E. ElMetwally [a,b,1], Jiuyan Chen [a], Wenquan Shi [c], Emel K. Cilingir [a], Brian Walters [d], Keenan J. Mintz [a], Christian Martin [a], Braulio C.L.B. Ferreira [a], Wei Zhang [a], Sajini D. Hettiarachchi [a], Leonardo F. Serafim [a], Patricia L. Blackwelder [a,e], Athula H. Wikramanayake [d], Zhili Peng [c,*], Roger M. Leblanc [a,*]

[a] Department of Chemistry, University of Miami, Coral Gables, FL 33146, USA
[b] Petrochemicals Department, Egyptian Petroleum Research Institute, Nasr City, Cairo 11727, Egypt
[c] National Center for International Research on Photoelectric and Energy Materials, School of Materials and Energy, Yunnan University, Kunming, Yunnan 650091, People's Republic of China
[d] Department of Biology, University of Miami, Coral Gables, FL 33146, USA
[e] MGS/RSMAS, University of Miami, Key Biscayne, FL 33149, USA

GRAPHICAL ABSTRACT

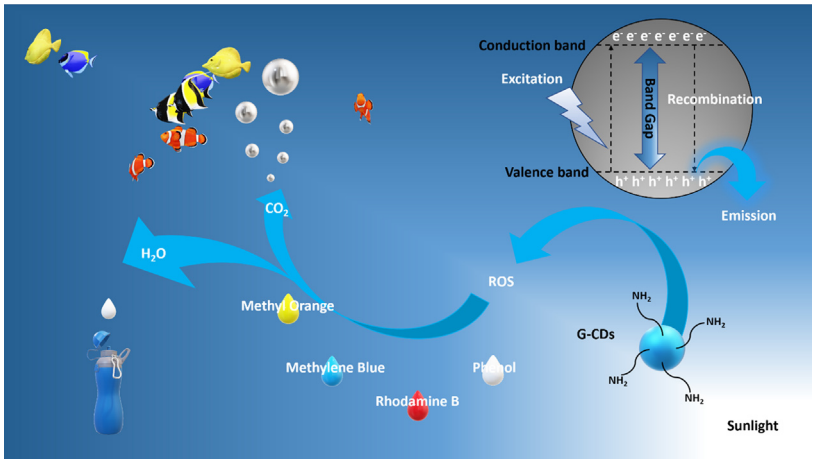

ARTICLE INFO

Article history:
Received 6 March 2021
Revised 16 April 2021
Accepted 26 April 2021
Available online 28 April 2021

Keywords:
Photocatalysis
Carbon dots
Wastewater treatment
Degradation

ABSTRACT

To protect water resources, halt waterborne diseases, and prevent future water crises, photocatalytic degradation of water pollutants arouse worldwide interest. However, considering the low degradation efficiency and risk of secondary pollution displayed by most metal-based photocatalysts, highly efficient and environmentally friendly photocatalysts with appropriate band gap, such as carbon dots (CDs), are in urgent demand. In this study, the photocatalytic activity of gel-like CDs (G-CDs) was studied using diverse water pollution models for photocatalytic degradation. The degradation rate constants demonstrated a remarkably enhanced photocatalytic activity of G-CDs compared with most known CD species and comparability to graphitic carbon nitride (g-C_3N_4). In addition, the rate constant was further improved by 1.4 times through the embedment of g-C_3N_4 in G-CDs to obtain CD-C_3N_4. Significantly, the rate constant was also higher than that of g-C_3N_4 alone, revealing a synergistic effect. Moreover,

* Corresponding authors.
E-mail addresses: zhilip@ynu.edu.cn (Z. Peng), rml@miami.edu (R.M. Leblanc).
[1] Both authors contribute equally to this work.

https://doi.org/10.1016/j.jcis.2021.04.121

Mineralization

the use of diverse radical scavengers suggested that the main contributors to the photocatalytic degradation with G-CDs alone were superoxide radicals ($O_2^{\cdot-}$) and holes that were, however, substituted by $O_2^{\cdot-}$ and hydroxyl radicals (·OH) due to the addition of g-C_3N_4. Furthermore, the photocatalytic stabilities of G-CDs and CD-C_3N_4 turned out to be excellent after four cycles of dye degradation were performed continuously. Eventually, the nontoxicity and environmental friendliness of G-CDs and CD-C_3N_4 were displayed with sea urchin cytotoxicity tests. Hence, through various characterizations, photocatalytic degradation and cytotoxicity tests, G-CDs proved to be an environmentally friendly and highly efficient future photocatalyst.

1. Introduction

Water covers 70% of the Earth's surface and 97% of it is present in the ocean. In the remaining 3%, 2% of water resides in glaciers and ice caps in the form of ice while fresh water only occupies less than 1% of all the water present on Earth [1]. To make things even worse, not all fresh water is drinkable. In fact, in some regions, particularly in the West and Southeast United States, the supplies of drinking water are dramatically low due to drought and aquifer depletion [2,3]. In many native reserves of Canada, clean drinking water is even considered as a luxury [4]. Additionally, fresh water, which includes drinking water, can be easily contaminated by human activities and natural disasters [5–7]. The year 2020 witnessed continuous natural disasters including Atlantic hurricanes, wildfires in the United States, Australia and the Amazon rainforest, as well as the COVID-19 pandemic. During or after these natural disasters, clean drinking water may become a most desirable but inaccessible resource [8]. The goal of this study is not only to call for the preservation of natural water resources but also to provide a novel solution to purify contaminated water and prevent future water pollution caused by chemicals and/or microorganisms to avoid accidents like the *Deepwater Horizon* oil spill in 2010 and Walkerton *E. coli* outbreak in 2000. Therefore, degradation of unwanted chemicals and organisms in water without harming the body of water is of great significance to the future access of clean water.

Photocatalytic degradation is a promising technology in water purification [9]. It utilizes sunlight and an appropriate photocatalyst to induce the generation of reactive oxygen species (ROS) from water and dissolved oxygen leading to the breakdown of organic pollutants [10]. Currently, common wastewater treatment methodologies include chemical oxidation, biological methods, combustion, flocculation, adsorption on granular activated carbon, air stripping, and precipitation [11]. In comparison with the aforementioned techniques, the biggest advantage of photocatalytic degradation is the complete mineralization of hazardous organic pollutants to water, carbon dioxide and simple mineral acids instead of converting them to secondary contaminants [12]. Additionally, photocatalytic degradation is efficient, low-cost and feasible at room temperature, which has enabled the removal of a wide range of organic water pollutants such as pesticides, herbicides, and micropollutants such as endocrine disrupting compounds [13–15]. Furthermore, the generated ROS have the ability to act on a broad spectrum of waterborne pathogenic microorganisms by causing direct oxidative damage, or by a variety of nonoxidative mechanisms including pattern recognition receptors (PRR) signaling, autophagy, neutrophil extracellular trap formation, and *T*-lymphocyte responses [16,17]. To be more specific, interactions between ROS and thiol groups in protein, DNA, and cell membrane of pathogens can induce their apoptosis [18]. Additionally, the most damaging ROS, hydroxyl radicals (·OH) can promote lipid peroxidation by triggering the chain oxidation of polyunsaturated phospholipids of bacterial cell membranes [19,20]. Moreover, hydrogen peroxide (H_2O_2)-dependent cytotoxicity arises with the interactions of DNA bases that break the deoxyribose chains [21]. In summary, photocatalytic degradation is a thorough and transformative water purification approach.

Currently, the biggest obstacle in the optimization of photocatalytic degradation processes is the design of appropriate photocatalysts. Due to many unique properties that result from nanoscale [22] nanomaterials have been widely studied for their photocatalytic activities, which include metal oxides (TiO_2, Fe_2O_3, ZnO, $BiVO_4$, etc.) [23–26], metal chalcogenides (CdS, ZnS, MoS_2, etc.) [27–29], metal-free nanomaterials such as graphitic carbon nitride (g-C_3N_4) [30] and their composites (Zn-CeO_2, Si-Ti, CdS-TiO_2, etc.) [31–34]. However, since the majority of present photocatalysts contain metals, their use will pose a risk of secondary pollution to the body of water [35]. In contrast, metal-free nanomaterials such as g-C_3N_4 are of great significance to environmental and ecological protections so their development deserves more attention [36–38]. Moreover, metal sulfides suffer from photocorrosion [39]. And even though metal oxides are generally stable in aqueous media, most of them possess large band gaps [40]. Band gap is one of the most important characteristic properties of a semiconductor [41]. It indicates the energy gap between the top of the valence band and the bottom of the conduction band [42] and it also represents an energy range where no electronic states exist [43]. However, the introduction of heteroatoms such as O, N, B, P, S [44] and related chemical bonds can add single or multiple electronic states between the valence and conduction bands, which usually results in the narrowing of band gap [45]. To be specific, in order to be a good photocatalyst, the nanomaterial should possess a band gap between 1.23 and 3.00 eV that will enable photocatalytic processes to utilize visible and infrared wavelengths which make up more than 90% of the overall solar radiation spectrum [46]. Thus, to obtain versatile photocatalysts, future design has to take into consideration many factors including the impact on environment and ecology, photocatalytic stability, and band gap.

Meanwhile, considering numerous favorable characteristics such as small size, high specific surface area, tunable surface functionality, benign biocompatibility, low toxicity and unique optical properties, carbon-based NPs including the aforementioned g-C_3N_4 are being rapidly developed in the hope of replacing toxic heavy metal-containing NPs in diverse application fields. Among various carbon-based nanomaterials, carbon dots (CDs) are a relatively new family member whose discovery can be traced back to the early 21st century [47]. Since then, there have been an increasing number of studies related to the synthesis, property characterization and application of CDs in the past two decades [48–51]. CDs have been observed to be spherical NPs with a mean diameter of between 1 and 10 nm. In terms of structure, CDs are compared with traditional quantum dots (QDs) and defined as core-shell nanostructures [52,53]. Also, CDs exhibit many unique properties that are rarely centered on any other known nanomaterials. For instance, different from many NPs, CDs can be directly obtained from food and beverage such as barbecued food [54] honey [55]

and beer [56] which reveals their good biocompatibility, low cost, and convincingly demonstrates their reliable uses in human or the environment. In addition, compared with traditional QDs and gold, silver, zinc oxide NPs, CDs are carbon-based NPs with no metallic toxicity. In comparison to liposomes, the mean diameter of CDs is much smaller allowing for a high surface-area-to-volume ratio, which is beneficial for their interactions with diverse contaminants in water. In contrast to carbon nanotubes, CDs are easier to synthesize with just a domestic microwave oven and short heating time [57]. CDs are also well characterized for their excellent light harvesting ability and photoluminescence (PL) properties [58–61]. Furthermore, due to abundant electron donors and acceptors present on the surface [62], CDs are promising photocatalysts [63]. Nonetheless, photocatalytic activities of CDs alone were not characterized in early studies and CDs were often coupled with those well-established photocatalysts such as Fe_2O_3 [64], TiO_2 [65–67], ZnO [68], SnS_2 [69], BiOBr [70], and g-C_3N_4 [71], to enhance their photocatalytic performances especially under visible light. It was not until 2017 that our research group initiated studies on photocatalytic activities of bare CDs which were found to be size-dependent [35]. Subsequently, in the past few years, the research on photocatalytic degradation of contaminants in water with CDs alone as photocatalysts is rapidly increasing, but the main challenge for translation of research into practical applications is the low degradation efficiency. Recently, a group of gel-like CDs (G-CDs) showed a tremendously high photocatalytic efficiency in the degradation of water contaminants, which might have achieved the highest performance of current CD-based photocatalysts to the best of our knowledge. Meanwhile, this finding also suggests that G-CDs might be another metal-free fundamental photocatalytic material like g-C_3N_4.

Herein, the photocatalytic activity of G-CDs has been extensively studied through data analysis of various degradation processes. In addition, G-CDs have been systematically characterized in our previous studies by UV/vis absorption, fluorescence emission, Fourier-transform infrared (FTIR), X-ray photoelectron spectroscopies (XPS), mass spectrometry (MS), thermogravimetric analysis (TGA), atomic force microscopy (AFM), transmission electron microscopy (TEM), and zeta potential measurement [72,73]. In this study, we only present a few important characterizations by UV/vis absorption, fluorescence emission, FTIR spectroscopies, X-ray powder diffraction (XRD), XPS, AFM and TEM. Moreover, the fluorescence quantum yield (QY) of G-CDs was measured with two standards for cross calibration. Then, the photocatalytic activity of G-CDs was evaluated by calculating the photocatalytic degradation rate constants of diverse organic dyes and phenol, a prevalent industrial effluent [74]. Each rate constant was compared with that for g-C_3N_4 and other CDs. Furthermore, in order to enhance the photocatalytic activity of G-CDs, g-C_3N_4 was incorporated in G-CDs to acquire the CD-C_3N_4 composite. In fact, combination of g-C_3N_4 and various NP species via composition and surface modification has generally shown a high photocatalytic activity in many applications due to the abundance of active sites and desired surface, which thus reduces the recombination of charge carriers and enhances the photocatalytic activity.[75–77] The CD-C_3N_4 was characterized and applied as the photocatalyst in the degradation of a wide spectrum of water contaminants whose rate constants were compared with that of g-C_3N_4 and G-CDs alone. Subsequently, the band gap of G-CDs and CD-C_3N_4 were measured by diffuse reflectance spectroscopy while the determination of ROS was conducted with a comprehensive radical scavenger test. Later, to test the photocatalytic stability of G-CDs and CD-C_3N_4, dye degradation with multiple cycles was performed. The cytotoxicity of G-CDs and CD-C_3N_4 were investigated by analyzing the survival rate of sea urchins.

2. Experimental

2.1. Materials

Citric acid (99.5–100%), acetone (99.9%) and quinine sulfate dihydrate (>99%) were bought from VWR (West Chester, PA). 1,2-ethylenediamine (EDA) (≥99.0%) was provided by MP Biomedicals (Irvine, CA). Harmane (>98%) and phenol (99+%) were ordered from Sigma-Aldrich (St. Louis, MO). Isopropanol alcohol (IPA) (99+%), *p*-benzoquinone (98+%), methylene blue (MB) (>95%), methyl orange (MO) (>95%), rhodamine B (RhB) (95%), and ethylenediaminetetraacetic acid disodium salt (EDTA-Na) (99%) were purchased from Alfa Aesar (Haverhill, MA). Compressed argon and nitrogen gases with ultra-high purity were acquired from Airgas (Miami, FL). Deionized (DI) water with resistivity of 18.2 MΩ·cm and surface tension of 72.6 mN m^{-1} was obtained via a Modulab 2020 water purification system (San Antonio, TX) at room temperature (20.0 ± 0.5 °C). All chemicals were used without further treatment.

2.2. Characterization

UV/vis absorption spectroscopy was performed using a UV/Vis spectrophotometer (Cary 100, Agilent Technologies, USA) and an optical cell with a 1-cm pathlength. A spectrofluorometer (Fluorolog-3, Horiba Jobin Yvon, USA) was applied to record fluorescence emission spectra with a slit width of 5 nm for both excitation and emission. FTIR spectroscopy was conducted on an FTIR spectrometer (Frontier, PerkinElmer, USA) equipped with attenuated total reflection (ATR) accessory. AFM was employed using an atomic force microscope (5420, Agilent Technologies, USA) with one drop of G-CDs, g-C_3N_4 or CD-C_3N_4 dispersion (1 mg/mL) transferred on a clean silica mica slide, which was followed by imaging with tapping mode. TEM was performed with a transmission electron microscope (1200×, JEOL, USA). A drop of G-CDs, g-C_3N_4 or CD-C_3N_4 dispersion (1 mg/mL) was placed on a carbon-coated 200 mesh copper grid and air dried. It is noteworthy that prior to both AFM and TEM screening, 5-min ultrasonication was applied to avoid self-aggregation. TGA of G-CDs, g-C_3N_4 and CD-C_3N_4 were conducted using a thermo-microbalance (TG 209 F3 Tarsus, Netzsch, USA) while heating under a flow of nitrogen gas from 40 to 1000 °C at a rate of 10 °C/min. XRD was performed using a diffractometer (TTRIII, Rigaku, Japan) equipped with Cu Kα radiation (λ = 1.5406 nm). XPS was measured on an XPS instrument (K-Alpha, Thermo Fisher Scientific, USA) with a monochromatic Al Kα source with a photon energy of 1486.6 eV, operated at 12 kV and 72 W. In the constant analyzer energy (CAE) mode of full spectrum scanning, the analyser pass energy was held constant at 100 eV with a step size of 1 eV while for narrow spectrum scanning, the pass energy was decreased to 50 eV with a step size of 0.1 eV. Calibration of binding energies was carried out with surface contamination C1s (284.8 eV) as the standard. To record the valence band spectrum, a pass energy 50 eV with a step size of 0.05 eV was applied. The corresponding binding energy calibration was carried out using surface contamination C1s (284.8 eV) as the standard.

2.3. Synthesis of G-CDs

To prepare G-CDs, first a 50-mL round-bottom flask was filled with argon gas for 5 min to expel O_2. Subsequently, 30 mL EDA was transferred to the flask and heated with constant stirring using an oil bath. When the temperature reached 160 °C, 6 g of citric acid was added to the flask. The reaction of citric acid and EDA proceeded for 50 min under the environment of argon gas for deaeration.[78] After the solvothermal system was cooled to room temperature, the G-CDs were deposited at the bottom of the flask

below the layer of unreacted EDA. To purify the G-CDs, unreacted EDA was removed with an acetone wash. (*Note:* In this study, the selection of an acetone wash instead of traditional CD purification methodologies such as dialysis and size exclusion chromatography was based on their G-CDs purification effects [79].) Finally, 10 g of G-CDs were dispersed in 100 mL DI water and heated by using a rotary evaporator (Bechi, R-114) to completely evaporate water, the remaining unreacted EDA and acetone at a constant temperature of 80 °C with reduced pressure until only G-CDs remained.

2.4. Assembly of CD-C_3N_4

Exfoliated g-C_3N_4 was prepared by following the procedures in the literature reference [80], and then incorporated in G-CDs during their syntheses. In detail, initially, 30 mL EDA was transferred to a 50-mL round-bottom flask previously filled with argon gas for 5 min. Subsequently, the round-bottom flask was heated with constant stirring using an oil bath. When temperature climbed up to 160 °C, 6 g of citric acid mixed with 50 mg of as-obtained g-C_3N_4 was added to the flask containing boiling EDA. The reaction lasted for 50 min under the environment of argon gas for deaeration.[78] After the solvothermal system was cooled down to room temperature, the g-C_3N_4-embedded G-CDs (CD-C_3N_4) were deposited at the bottom of the flask below the layer of unreacted EDA. The purification of CD-C_3N_4 followed the same procedures for G-CDs but the physical appearance of CD-C_3N_4 was different from that of G-CDs alone, which is exhibited in **Fig. S1** in the supporting information.

2.5. Fluorescence quantum yield calculation

The fluorescence QY of as-prepared G-CDs was calculated with the absorbance at 350 nm and the integrated PL intensity obtained at the excitation of 350 nm using both quinine sulfate dihydrate and harmane as reference standards. It is well known that quinine sulfate and harmane in 0.1 M H_2SO_4 aqueous solution possess a fluorescence QY of 54 and 83%, respectively [81,82]. The absorbances of two standards and G-CDs were acquired with three runs each in a quartz cuvette with a 1-cm pathlength. In addition, the concentrations of two standards and G-CDs have to be well adjusted to ensure the absorbance at 350 nm lower than 0.05. Then, the fluorescence emission spectra of the same solutions were recorded three times each under the excitation of 350 nm. The average of absorbances and integrated PL intensities were taken into the following equation:

$$\Phi = \Phi_R \times (I / I_R) \times (A_R / A) \times (\eta^2 / \eta_R^2)$$

In this equation, Φ, I, A and η represent fluorescence QY, integrated PL intensity, absorbance at 350 nm, and refractive index of water which is 1.33 [83], respectively. Subscript R is denoted for the reference.

2.6. Photocatalytic degradation of organic pollutants

All photocatalytic degradation experiments were carried out in a quartz cuvette with a 1-cm pathlength placed 10 cm in front of a solar simulator (Oriel Instruments, Newport Corporation) equipped with a high-power mercury-xenon light source (see **Fig. S2** in the supporting information for the spectrum). The cuvette had been filled with 4 mL of aqueous solution (10 mg L^{-1}) of each dye and 12 mg of G-CDs or CD-C_3N_4. The used dyes included RhB, MB and MO. G-CDs or CD-C_3N_4 was ultrasonically dispersed in various dye solutions. Photocatalytic reactions were initiated by switching on the lamp, adjusting the power to 310 W and recording the initial absorbances at 554 (RhB), 664 (MB) and 464 nm (MO). Subsequently, in order to keep the concentration of photocatalysts and pollution models steady throughout the whole UV/vis absorption measurement, instead of measuring out a few aliquots of samples, we directly used the cuvette containing both photocatalyst and pollution model for UV/vis absorption measurement, so the sample volume used for this purpose was constantly 4 mL. Absorbances were read out every 10 min by the UV/vis spectrophotometer. According to the Beer-Lambert law, the absorbances reflect on the concentration changes of each dye. Furthermore, phenol degradation was conducted by following the same procedures. However, due to overlap of absorption peaks of G-CDs, CD-C_3N_4 and phenol, the phenol degradation extent was monitored at the retention time of 3.25 min on an HPLC (Dionex UltiMate 3000) equipped with Dionex UltiMate 3000 diode array detector and Agilent Eclipse Plus C18 column (3.5 μm × 4.6 × 100 mm). The flow rate of the mobile phase (CH_3CN:H_2O = 30:70, v/v) was adjusted to 1 mL min^{-1} during the analysis. Shimadzu TOC-L analyzer was used to monitor the extent of mineralization after photocatalytic reactions. All experiments were conducted at least three times each, unless mentioned otherwise, to ensure the accuracy and reproducibility of our results.

2.7. Cytotoxicity studies of G-CDs and CD-C_3N_4

Sea urchins were employed to test the cytotoxicity of G-CDs and CD-C_3N_4. Sea urchins (*Lytechinus variegatus*) were acquired from the Duke University Marine Lab (Beaufort, NC, U.S.A). Sea urchins are invertebrates and as such research with these animals do not require specific ethical care permits. The animal care protocol for all procedures used in this study was approved by the University of Miami Animal Care and Use Committee and complies with the guidelines of the National Science Foundation. Fertilized sea urchin eggs were grown in a 24-well plate. 100 embryos were placed in each well with 200 μL of filtered seawater. Then, the embryos were separately treated with different concentrations (0, 10, 25, 100 μM) of G-CDs and CD-C_3N_4 dispersed in 400 μL of seawater and incubated at 21 °C. After 24 h post fertilization at the gastrula stage of sea urchin development, survival rates of the sea urchin embryos were measured with three biological replicates. Significance of sea urchin cytotoxicity studies were determined using Student's t-tests for all pairwise comparisons of the different treatments that were tested. All the results are mentioned as the mean ± standard error of the mean (SEM). Significance was set at $p < 0.05$.

3. Results and discussion

The G-CDs in our study have a high product yield and can be rapidly produced on large scale in one-pot hydrothermal reaction which can be easily deactivated in a round-bottom flask and oil bath. To be specific, within 1 h, 10 g of G-CDs can be produced from 6 g of citric acid and 30 mL EDA. Compared with many CD species and nanomaterials in general, to the best of our knowledge, the product yield is honestly good for industrial production. In addition, the excess of EDA can be reused to save the expense.

3.1. Characterizations of G-CDs and CD-C_3N_4

In this study, UV/vis absorption, fluorescence emission, FTIR spectroscopies, AFM and TEM were applied to briefly refresh the optical properties, structure and morphology of G-CDs. In the UV/vis absorption spectrum of G-CDs (Fig. 1**a**), it is clear that G-CDs consist of C=C (245 nm) and C=O/C=N (287–335 nm) structures. Based on the fluorescence emission spectra as well as corresponding normalized spectra (Fig. 1**b**), G-CDs possess an

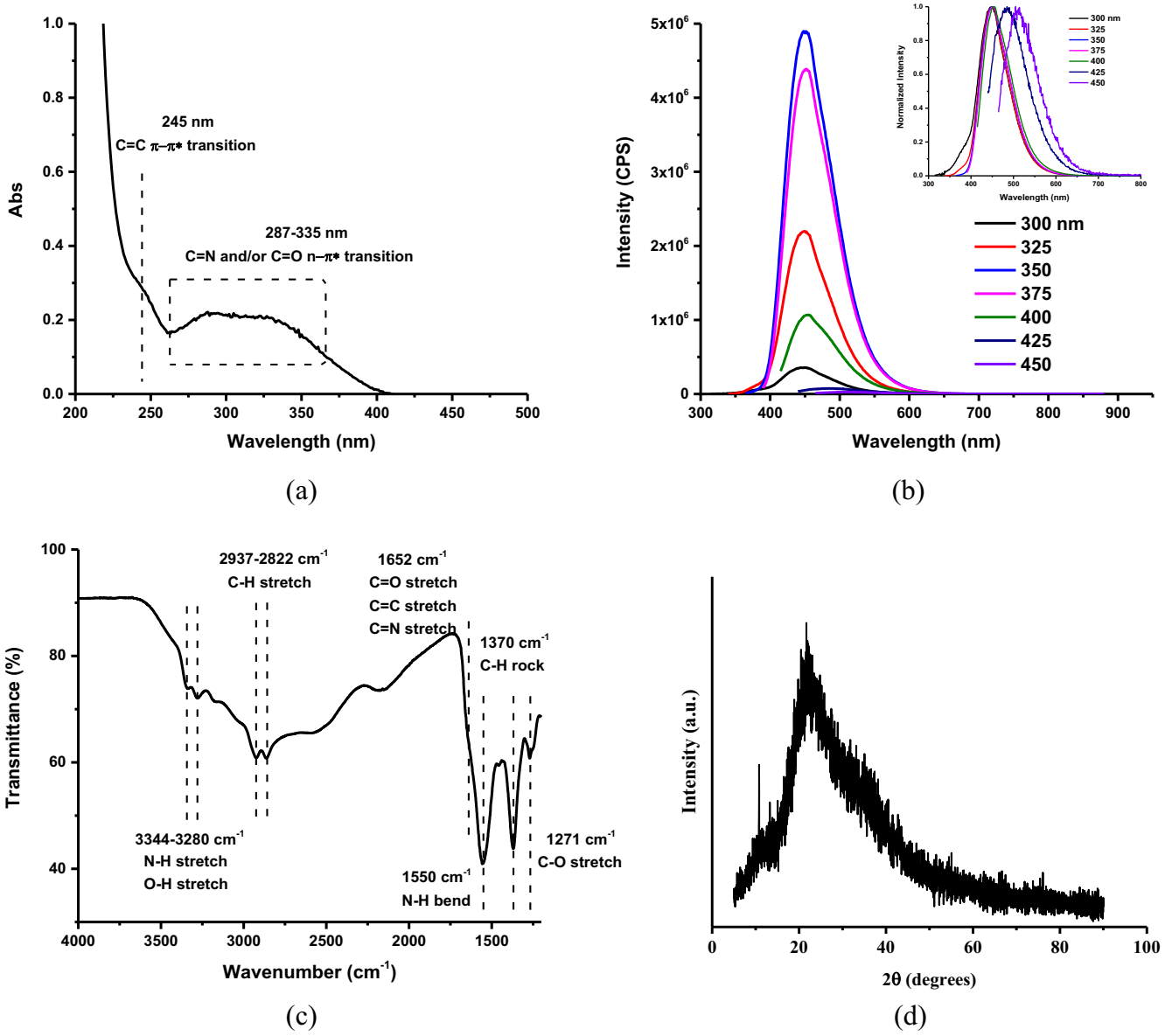

Fig. 1. Brief physicochemical characterizations of G-CDs. (a) UV/vis absorption spectrum of G-CDs in aqueous medium (0.9 mg/mL); (b) fluorescence emission spectra of G-CDs in aqueous medium (0.01 mg/mL) with the normalized spectra as inset; (c) FTIR spectrum of G-CDs in gel state with air as background; (d) XRD of G-CDs; (e) XPS spectra; (f) XPS C1s spectra; (g) O1s spectrum; (h) N1s spectra of G-CDs; (i) AFM and (k) TEM images of G-CDs with particle size distribution histogram as inset. The scale bar in the TEM image represents 10 nm.

excitation-dependent PL and the maximum excitation and emission wavelengths are 350 and 450 nm, respectively. In addition, to calculate the fluorescence QY of G-CDs, quinine sulfate and harmane were selected as two reference standards considering their similar PL behaviors to G-CDs. Cross calibrations were conducted and the fluorescence QY of quinine sulfate (literature: 54% [84]) and harmane (literature: 83% [85]) was measured as 55 and 81.5%, respectively. Based on these results, it can be concluded that our methodology was reliable. Thereafter, the fluorescence QY of G-CDs was measured to be 42% using both reference standards. As to the determination of functional groups on G-CDs, FTIR spectrum (Fig. 1**c**) reveals $-NH_2$ and/or –OH stretch (3344–3280 cm^{-1}), C—H stretch (2937–2822 cm^{-1}), C=O/C=N/C=C stretch (1652 cm^{-1}), N—H bend (1550 cm^{-1}), C—H rock (1370 cm^{-1}) and C—O stretch (1271 cm^{-1}) [72]. Among them, the presence of $-NH_2$ and –OH ensures a good water dispersity of G-CDs. More importantly, the peaks indicating $-NH_2$ stretch (3344–3280 cm^{-1}) and C—H stretch (2937–2822 cm^{-1}) were confirmed by the FTIR spectrum of EDA [86], which demonstrates the successful condensation polymerization reaction between citric acid and EDA. Moreover, the XRD pattern (Fig. 1**d**) of G-CD shows a wide peak at 25°, which is caused by highly disordered carbon atoms [87]. XPS of G-CDs (Fig. 1**e**) reveals 61.48% of carbon, and 21.07% of oxygen, and 17.45% of nitrogen. In the C1s core levels (Fig. 1**f**), the binding energies at 284.6, 286.1 and 287.6 eV were assigned to C—H/C—C, C—O—C, and C=O, respectively [88]. The O1s core level (Fig. 1**g**) showed a narrow peak at 531 eV, which was presumed to be C=O.[72] In the N1s spectrum (Fig. 1**h**), the binding energies at 399.0 and 400.8 eV were ascribed to C=N and $-NH_2$, respectively.[35,72]

The AFM image in Fig. 1**d** exhibits plenty of spherical-shaped nanostructures of G-CDs with a mean size of 1.6 nm along the z-axis. Meanwhile, the TEM image in Fig. 1**e** shows an even distribution of G-CDs on the copper grid, which suggests that G-CDs have a high water-dispersity and aqueous stability. In addition, according to the narrow size distribution revealed by the TEM size distribu-

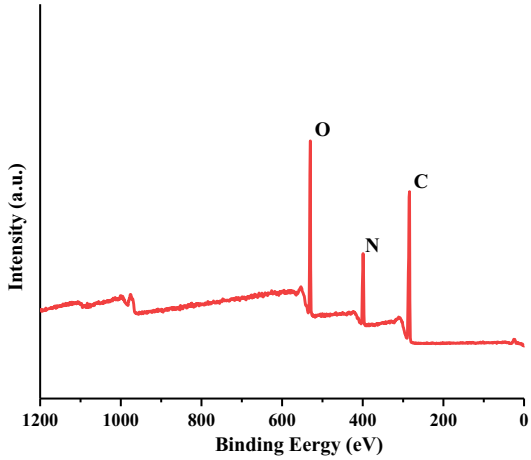

(e)

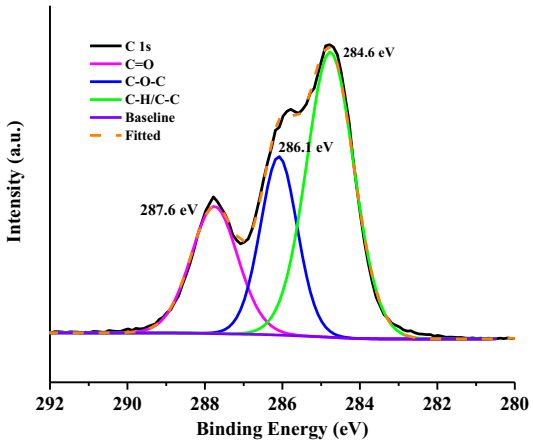

(f)

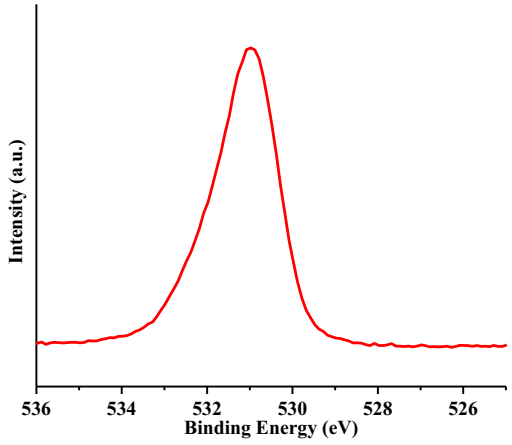

(g)

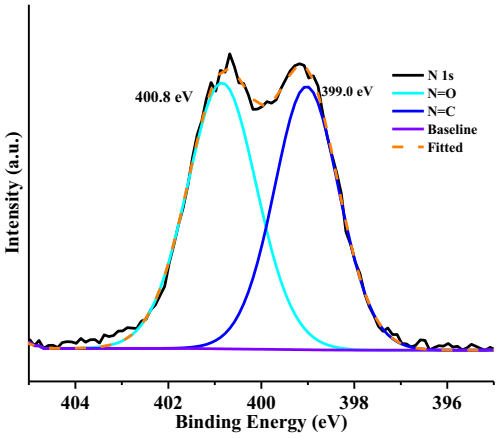

(h)

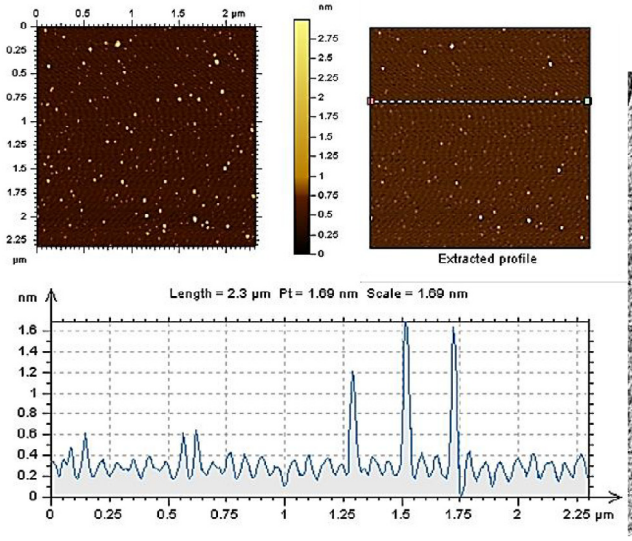

(i)

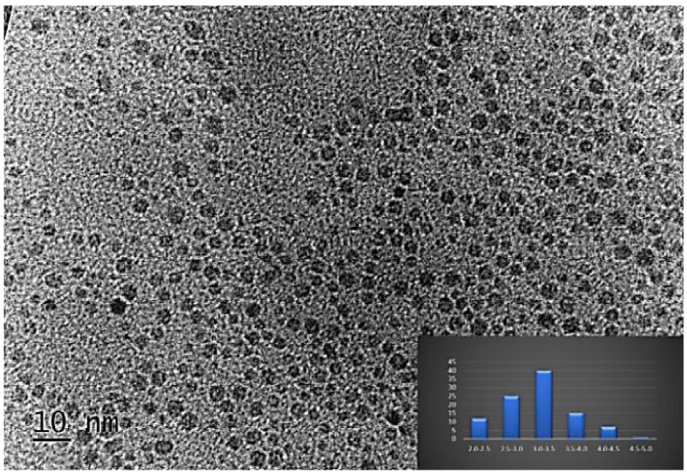

(k)

Fig. 1 (*continued*)

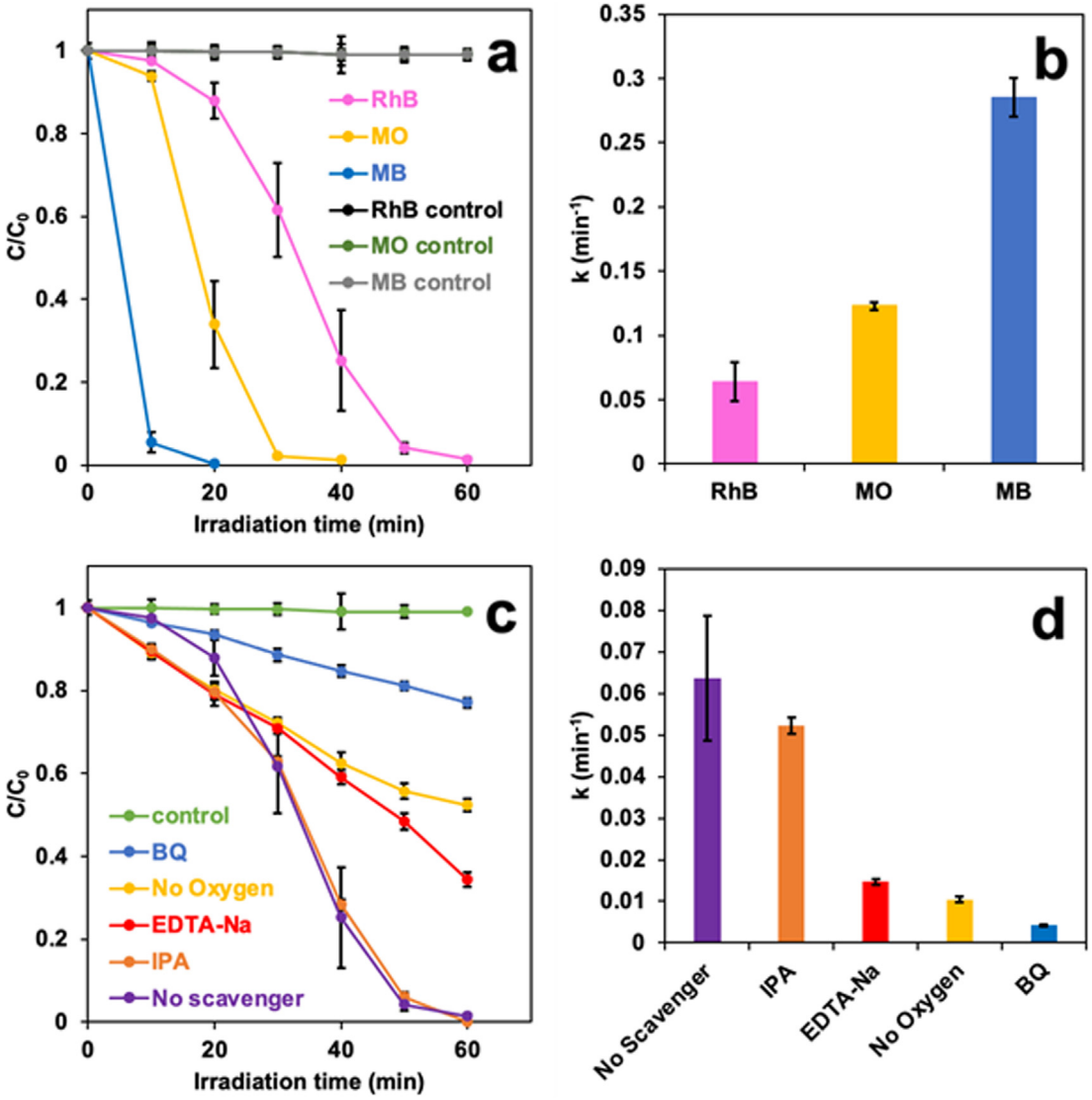

Fig. 2. (a) Photocatalytic degradation with G-CDs as the photocatalyst and (b) pseudo-first-order rate constants of different dyes. (c) Photocatalytic degradation with G-CDs as the photocatalyst and (d) pseudo-first-order rate constants of RhB degradation in the presence of IPA, benzoquinone, EDTA-Na, and no scavenger. Conditions: initial dye concentration (10 mg L^{-1}), photocatalyst weight (12 mg), light power (310 W), pH (neutral) and temperature (20 °C). Controls refer to photodegradation of dyes in the absence of G-CDs. All experiments were conducted at least three times each.

tion histogram, the mean size of G-CDs in the xy-plane is 3.2 ± 0. 5 nm. Thus, G-CDs are oval in shape.

CD-C_3N_4 was characterized by FTIR spectroscopy, XRD, XPS, TGA, AFM and TEM and strong supports for the assembly of G-CDs and g-C_3N_4 were provided by XRD, AFM and TEM images. The XRD patterns (**Fig. S3c**) demonstrate that CD-C_3N_4 has a wider peak at 25° than G-CD, which can be attributed to the doping of g-C_3N_4 [89]. In the XPS analysis of CD-C_3N_4, CD-C_3N_4 showed slight differences from G-CDs in the proportions of each element. For instance, XPS of G-CDs (Fig. 1**e**) reveals 61.48%, 21.07%, and 17.45% for carbon, oxygen and nitrogen, respectively. However, XPS spectra of CD-C_3N_4 (**Fig. S3d-g**) reveals 60.33% of carbon, 21.87% of oxygen, and 17.80% of nitrogen, which reveals a majority of G-CDs in CD-C_3N_4. In comparison to the morphology of g-C_3N_4 alone (**Fig. S3h and S3j**), AFM and TEM images of CD-C_3N_4 (**Fig. S3i and S3k**) show a few particles on the edge or surface of a g-C_3N_4 monolayer. However, since the majority of CD-C_3N_4 was G-CDs (99.5% by mass), no clear difference was observed between G-CDs and CD-C_3N_4 based on FTIR and TGA spectra (**Fig. S3a and S3b**). Nonetheless, they demonstrate a noncovalent interaction between G-CDs and g-C_3N_4 in the CD-C_3N_4 composite.

3.2. Photocatalytic degradation of organic pollutants

3.2.1. Degradation of organic dyes

When CDs were applied in photocatalytic degradation, the most common pollution model was chosen from various organic dyes. Nonetheless, the dye species are usually limited to 1–2 with either positive or negative charges, which lacks generalization. In comparison, in our study, the photocatalytic reactivity of as-prepared G-CDs was evaluated by degrading both negatively and positively charged dyes. To be specific, MO represents the negatively charged dye while RhB and MB represent the positively charged counterparts. To rule out the probability of dye degradation by photolysis, each dye was irradiated in the absence of G-CDs for 1 h as controls and the dye degradation extent was recorded and presented in Fig. 2**a**. It is evident that photolysis was incapable to degrade any of the tested dyes even after 1 h of irradiation, which highlights

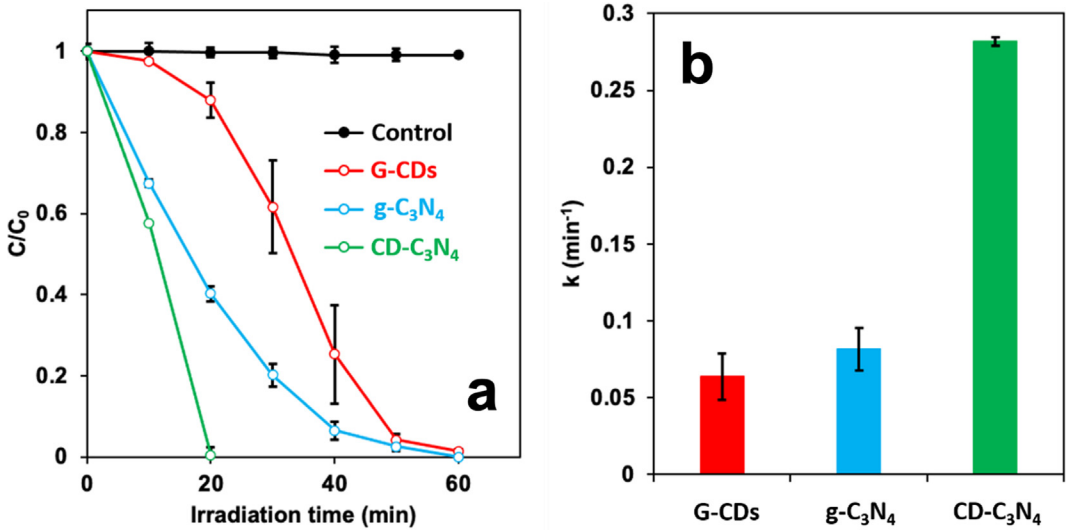

Fig. 3. (a) Photocatalytic degradation and (b) pseudo-first-order rate constants of RhB using different photocatalysts. Conditions: dye concentration (10 mg L^{-1}), photocatalyst weight (12 mg) unless mentioned otherwise, light power (310 W), pH (neutral), temperature (20 °C). Control refers to photodegradation of RhB in absence of any added photocatalyst. All experiments were conducted at least three times each.

the significant role of as-prepared G-CDs in the photocatalytic degradation of dyes. Next, the photocatalytic system (12 mg of G-CDs in 4 mL of each dye) was irradiated using a solar simulator while the absorbance at the aforementioned characteristic absorption peak of each dye was measured every 10 min and the obtained A/A_0 equal to C/C_0 are presented in Fig. 2**a**. The data reveal a substantial performance as the G-CDs were able to completely degrade all the three dyes after only 20, 40 and 60 min for MB, MO and RhB, respectively.

The photocatalytic degradation rate constants of the three dyes can be arranged as (k_{MB}) > (k_{MO}) > (k_{RhB}) with values of 0.29, 0.12 and 0.06 min^{-1}, respectively. Such high degradation rates displays the extraordinary photocatalytic reactivity of G-CDs towards degradation of the tested dyes especially when they were compared to the degradation rates achieved with other CD species as photocatalysts. Particularly, when 12 mg of the CDs (fraction 3 with the best performance) developed in our previous work [35] were applied in this work with all other parameters the same for G-CDs, their photocatalytic performance of RhB degradation was recorded in **Fig. S4** in the supporting information with a rate constant of 0.02 min^{-1}. In contrast, the RhB degradation rate constant was enhanced by 300% with G-CDs. In addition, Bhati *et al.* reported that red-emitting magnesium-nitrogen-embedded CDs were able to degrade MB with a rate constant of 0.04 min^{-1} [10]. Araújo *et al.* found that their hydrophilic CDs were capable to degrade indigo carmine dye with a rate constant of 0.0014 min^{-1} [90]. Li *et al.* analyzed the photocatalytic performance of their CDs in the degradation of MB, which yielded a rate constant of 0.0030 min^{-1} [91]. Zhu *et al.* discovered that the rate constants of RhB and MB degradations using biomass-derived CDs co-doped with S/Cl are 0.027 and 0.064 min^{-1}, respectively [92]. Ma *et al.* reported a type of *N*-doped CDs that could degrade 90% of MO after 120 min of visible light irradiation without any surface modification [93]. Thus, in comparison with all the CD species introduced above, our as-prepared G-CDs exhibited superior photocatalytic performance. Furthermore, it is worth noting that the degradation rates for G-CDs are comparable to those obtained for metal-free heterogenous photocatalysts such as g-C_3N_4. For instance, Yuan *et al.* reported that the photocatalytic degradation rate constants of RhB were 0.0087 and 0.0358 min^{-1} for bulk g-C_3N_4 and thermally exfoliated g-C_3N_4, respectively [94]. Such results prove that the as-prepared G-CDs are a potential alternative for traditional heterogenous photocatalysts in remediation of hazardous contaminants in wastewater effluents.

To identify the ROS responsible for the photocatalytic performances of G-CDs, photocatalytic experiments were conducted in presence of diverse radical traps while collecting the reaction rates. In detail, EDTA-Na, *p*-benzoquinone and IPA were used to trap holes, $O_2^{\cdot-}$ and ·OH, respectively. When the photocatalytic experiment was conducted in the presence of IPA, there was no noticeable change in the degradation extent of RhB (Fig. 2**c**) but with a slight reduction in the degradation rate (Fig. 2**d**). These results also ruled out the possibility of water oxidation via the generated holes. Nonetheless, when EDTA-Na was added, the degradation rate started to dwindle, reflecting the noteworthy contribution of holes to the degradation of RhB. Moreover, it is evident that the addition of *p*-benzoquinone as a $O_2^{\cdot-}$ trap, significantly hampered the degradation of RhB, which could be ascribed to the dominant role of $O_2^{\cdot-}$ in the degradation mechanism using the as-prepared G-CDs as photocatalysts.

To validate the dominant role of $O_2^{\cdot-}$, the photocatalytic degradation of RhB was carried out in the absence of dissolved oxygen by flushing the reaction medium with an ultrapure nitrogen flow for 1 h prior to initiating the reaction. Next, the nitrogen environment was maintained during the reaction via a nitrogen-filled balloon to simulate anerobic conditions. The data showed a substantial reduction in the degradation rate of RhB in comparison to aerobic conditions, indicating the crucial role of dissolved oxygen as an electron acceptor for $O_2^{\cdot-}$ generation. Moreover, it has been reported that illumination of RhB molecules generated RhB* radicals [95]. These radicals could facilitate electron transfer from the valance to conduction band of the photocatalyst, which in turn enhanced the degradation performance of the system [95].

To foster the photocatalytic reactivity, exfoliated g-C_3N_4 was incorporated into the as-prepared G-CDs and the performance of the CD-C_3N_4 composite was assessed by the photocatalytic degradation of RhB. The obtained results (Fig. 3) reveal that the addition of g-C_3N_4 markedly enhanced the photocatalytic performance of G-CDs in the degradation of RhB. To be specific, the complete degradation of RhB was achieved by CD-C_3N_4 after only 20 min of irradiation with a rate constant 4.5-fold higher than that of pristine G-CDs. For comparison, the performance of bare g-C_3N_4 was also evaluated in RhB degradation using a concentration equivalent to that used for preparation of CD-C_3N_4 and the obtained data are dis-

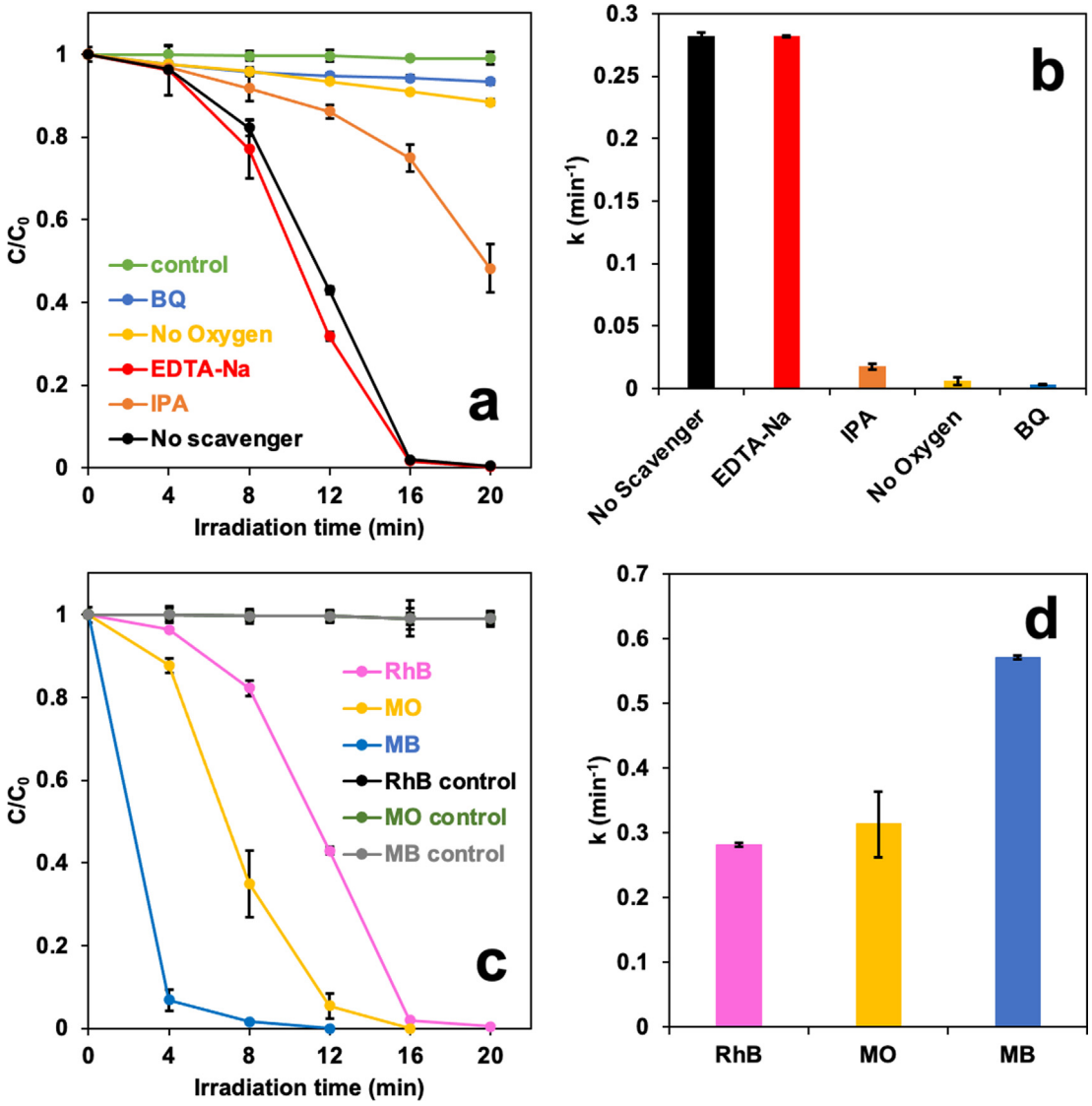

Fig. 4. (a) Photocatalytic degradation with CD-C_3N_4 as the photocatalyst and (b) pseudo-first-order rate constants of RhB in the presence of IPA, benzoquinone, EDTA-Na, and no scavenger. (c) Photocatalytic degradation with CD-C_3N_4 as the photocatalyst and (d) pseudo-first-order rate constants of different dyes. Conditions: initial dye concentration (10 mg L^{-1}), photocatalyst weight (12 mg), light power (310 W), pH (neutral), temperature (20 °C). Controls refer to photodegradation of dyes in the absence of CD-C_3N_4. All experiments were conducted at least three times each.

played in Fig. 3. It is clear that the degradation rate constant achieved by CD-C_3N_4 was 3-fold higher than that of pristine g-C_3N_4, demonstrating an outstanding performance, which was attributed to a synergy between g-C_3N_4 and G-CDs.

Such synergy was capable to enhance the production of active radicals that in turn, boost the degradation performance of the system. Those active radicals were identified by carrying out a series of radical trap experiments as presented in Fig. 4. The data show that the addition of IPA markedly inhibited the degradation of RhB, indicating the notable role of ·OH produced within the system. It is evident that the introduction of g-C_3N_4 to G-CDs was the reason behind the generation of ·OH as the G-CDs were incapable to produce such radicals. Nevertheless, it has been reported that the holes in the valence band of g-C_3N_4 were unable to oxidize either adsorbed water molecules or surface hydroxyl groups for ·OH generation [96]. Other reports suggested that those ·OH could be produced as a result of the reaction of $O_2^{\cdot-}$ with water molecules [97].

In addition, when *p*-benzoquinone was introduced to the system, the degradation rate declined to a substantial level, elaborating the dominant role of $O_2^{\cdot-}$. This dominant role was also validated using the data obtained from the anerobic photocatalytic experiments as discussed earlier. The degradation rate obtained in the absence of dissolved oxygen resembled that obtained in the presence of *p*-benzoquinone, indicating the pivotal role of dissolved oxygen as an electron acceptor for $O_2^{\cdot-}$ generation. For the EDTA-Na trap experiment, the results showed that the addition of EDTA-Na had almost no effect on the degradation rate of RhB as shown in Fig. 4**b**, indicating the inability of the generated holes to oxidize RhB molecules upon the introduction of g-C_3N_4 to G-CDs.

The photocatalytic reactivity of CD-C_3N_4 was also tested in the degradation of MB and MO, and the data (Fig. 4**c**) reveal that the degradation of MB was much faster than that of MO and RhB, where the complete degradation of MB and MO were achieved at 12 and 16 min, respectively. The rate constants for photocatalytic degradation of the three dyes can be arranged as (k_{MB}) > (k_{MO}) > (k_{RhB}) with values of 0.57, 0.31 and 0.28 min^{-1}, respectively. These findings reveal the ability of CD-C_3N_4 to remediate the negatively and positively charged dyes. The rate constants of photocatalytic degradation of the tested dyes (Fig. 4**d**) also manifest that the

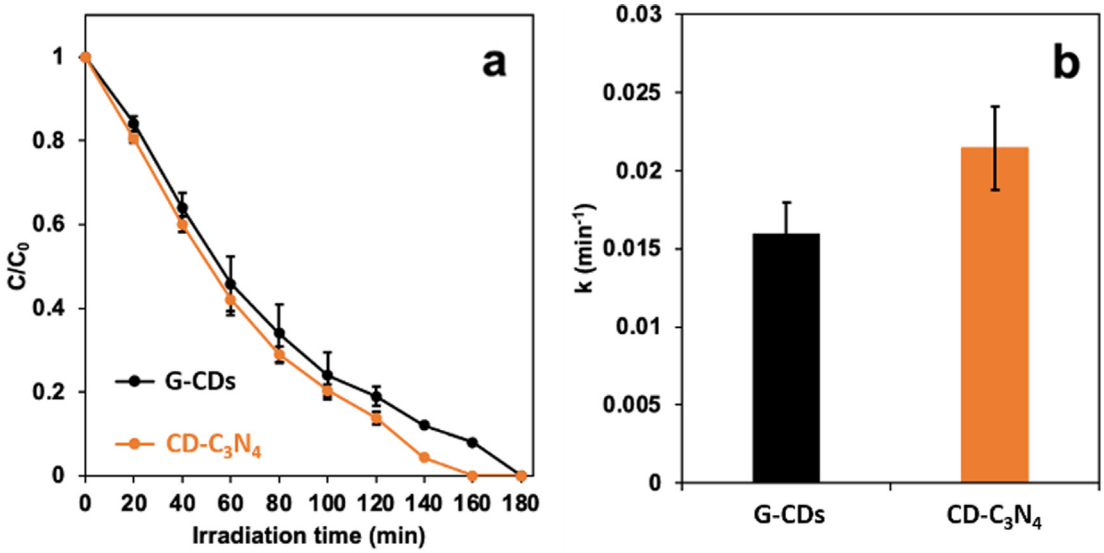

Fig. 5. Photocatalytic degradation of phenol using G-CDs and CD-C_3N_4 as separate photocatalysts. Conditions: initial phenol concentration (10 mg L^{-1}), photocatalyst weight (12 mg), light power (310 W), pH (neutral) and temperature (20 °C). All experiments were conducted at least three times each.

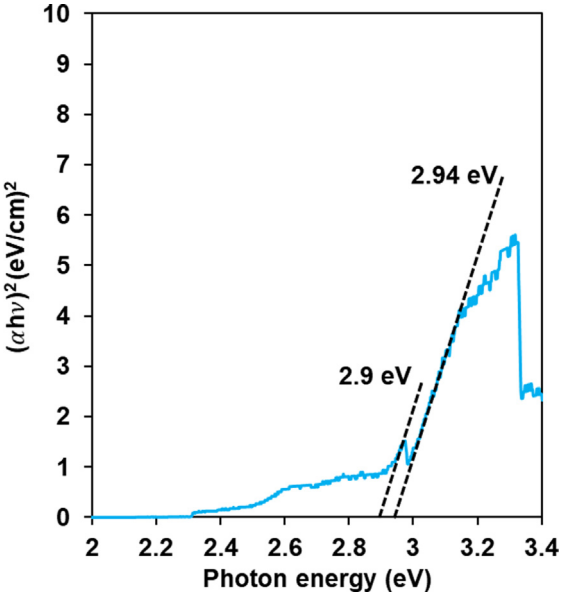

Fig. 6. Diffuse reflectance spectroscopy of CD-C_3N_4 in gel state. Plot of $(\alpha h\upsilon)^2$ vs. photon energy for CD-C_3N_4.

degradation rate was independent of the surface charge of CD-C_3N_4.

To examine the ability of CD-C_3N_4 to mineralize the tested dyes into carbon dioxide and water instead of converting them into toxic intermediates, total organic carbon (TOC) analysis was carried out before and after 60 min of irradiation for the three tested dyes. The obtained data (**Fig. S5**) reveal that the extent of TOC removal reached 71, 53.8 and 36% for MB, RhB and MO, respectively. Thus, it is evident that the employed system was capable of mineralizing the organic dyes into carbon dioxide and water. However, the incomplete mineralization implies that more drastic and/or longer treatments are required to entirely mineralize the tested dyes. The mineralization extent for the three tested dyes can be arranged as MB > RhB > MO, which can be ascribed to the surface interaction between the CD-C_3N_4 and the three tested dyes where the surface charge of CD-C_3N_4 was measured to be −4.7 mV.

3.2.2. Degradation of phenol

In addition to dyes, as a prevalent industrial effluent, phenol was also applied as a colorless contaminant model to investigate the photocatalytic performance of both G-CDs and CD-C_3N_4 in the treatment of industrial wastewater. Phenol is used primarily in the production of phenolic resins and in the manufacture of nylon and other synthetic fibers [98,99]. Severe exposure to phenol can cause kidney and/or liver damage, tremors, skin burns, twitching and convulsions [100]. Every day, a considerable amount of phenol enters the environment and the presence of such hazardous contaminant in the environment can markedly threaten human health. For phenol degradation experiments, 12 mg of G-CDs or CD-C_3N_4 was ultrasonically dispersed in 4 mL of phenol stock solution. Next, the system was irradiated using a solar simulator and the degradation extent was monitored using HPLC (Fig. 5). The data shows that phenol was completely degraded after 160 and 180 min of irradiation in the presence of CD-C_3N_4 and G-CDs, respectively. It is evident that the introduction of g-C_3N_4 enhanced the degradation rate of phenol (Fig. 5**b**) with rate constants of 0.021 and 0.015 min^{-1} for CD-C_3N_4 and G-CDs, respectively. The extent of phenol mineralization was also investigated using TOC analysis and the results showed that almost 90% of phenol was mineralized into carbon dioxide and water using the as-prepared CD-C_3N_4 as photocatalysts after 3 h of irradiation. Such data highlight the outstanding performance of CD-C_3N_4 in degradation and mineralization of a wide spectrum of water contaminants.

3.3. Band gap measurement

As a green substitute for traditional semiconducting QDs, except for the core-shell nanostructure, CDs also possess many properties similar to that of semiconducting QDs such as valence, conduction bands and a moderate band gap suitable for many photocatalytic activities. In this study, the band gap of G-CDs was measured by diffuse reflectance spectroscopy as 2.94 eV which was close to that (2.9 eV) of as-prepared exfoliated g-C_3N_4 as indicated by **Fig. S6**. In addition, it reveals the absorption band edge of G-CDs at 420 nm, which signifies that G-CDs are able to utilize both UV and visible lights for photocatalytic activities. Furthermore, the diffuse reflectance spectrum of CD-C_3N_4 (Fig. 6) shows the coexistence of the band gaps of G-CDs and g-C_3N_4, which confirms

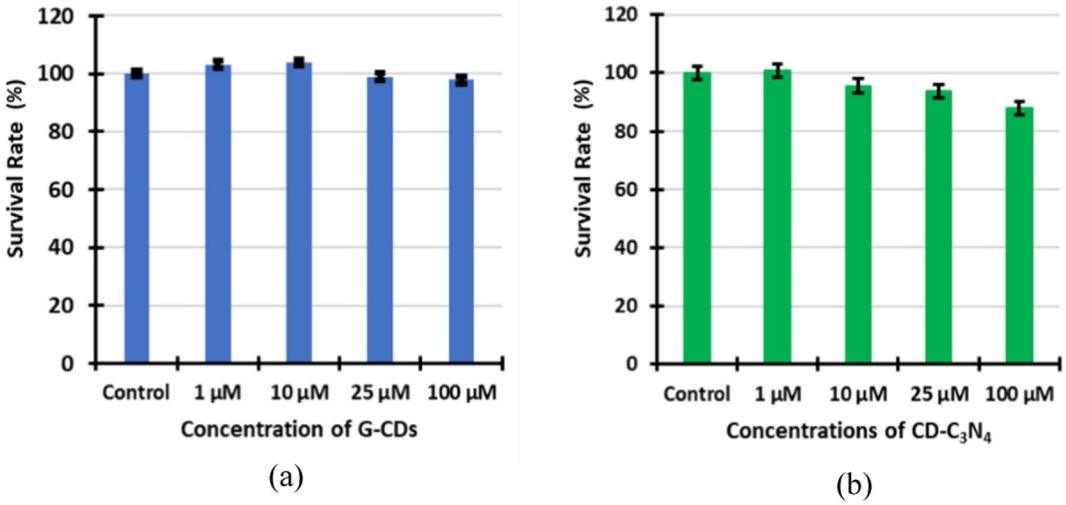

Fig. 7. Sea urchin cytotoxicity studies for a) G-CDs and b) CD-C_3N_4 at varying concentrations. All experiments were conducted at least three times each.

the aforementioned noncovalent interaction between G-CDs and g-C_3N_4 in the CD-C_3N_4 composite. Based on these results, the as-prepared G-CDs and CD-C_3N_4 can be considered as direct semiconductors with appropriate band gap for photocatalytic reactions. Nonetheless, the band gap of G-CDs and CD-C_3N_4 are still large, which can be optimized by introducing heteroatoms such as O, N, B, P, S during their syntheses with appropriate precursors or after their syntheses with proper surface modifications.

3.4. 3.4. Photocatalytic stability test

G-CDs and CD-C_3N_4 were tested for their photocatalytic stabilities via RhB degradation. Initially, RhB underwent a regular photocatalytic degradation in the presence of G-CDs or CD-C_3N_4. After 60 min (G-CDs) or 20 min (CD-C_3N_4) when the majority of RhB was degraded, the same solution containing G-CDs or CD-C_3N_4 was exposed to the simulated sunlight for 20 min to completely degrade RhB residues. Subsequently, 200 μL of fresh RhB solution (0.2 mg/mL) was added to the solution containing G-CDs or CD-C_3N_4 and irradiated by the solar simulator. The UV/vis absorption spectrum was recorded every 15 and 4 min for G-CDs and CD-C_3N_4, respectively until the peak at 554 nm disappeared. These processes were repeated two more times. **Fig. S7** records the RhB degradation over time for evaluation of the photocatalytic stability of G-CDs and CD-C_3N_4. After four cycles of RhB degradation, based on their constant degradation rates, no significant decrease was observed in the photocatalytic activities of G-CDs and CD-C_3N_4. Also, after exposure to sunlight for 2 h, G-CDs were characterized by UV/vis absorption, fluorescence emission and FTIR spectroscopies. The results were presented in the supporting information as **Fig. S8** and no appreciable differences were observed before and after long time of irradiation. Meanwhile, since the majority of CD-C_3N_4 is G-CDs, no additional characterizations were performed on CD-C_3N_4 after 2 h of irradiation by the solar simulator. Therefore, it can be concluded that both G-CDs and CD-C_3N_4 have excellent photocatalytic stabilities.

3.5. Cytotoxicity studies of G-CDs and CD-C_3N_4

Sea urchins were selected as an *in vivo* model in this study to investigate the cytotoxicity of G-CDs and CD-C_3N_4 considering its acute toxic sensitivity [101]. As shown in Fig. 7**a and 7b**, more than 87% of the sea urchin embryos maintained their normal development even in the presence of high concentrations of G-CDs or CD-C_3N_4 such as 100 μM. In addition, $P > 0.05$ so there was no significant difference from % survival rate of control groups. In other words, there was no significant difference observed between the survival rates of the control group and both CDs' treatments. Thus, it can be concluded that both G-CDs and CD-C_3N_4 have good biocompatibility and very low cytotoxicity towards sea urchin embryos at the tested concentrations.

Therefore, given the high photocatalytic reactivity of both photocatalysts, their negligible impact on the ecology upon the purification of wastewater is going to enable their wide applications in real life. In addition, since both photocatalysts will not harm the environment or human health, the collection of both photocatalysts after use is not necessary.

4. Conclusion

In conclusion, G-CDs exhibit a substantial photocatalytic activity in comparison with most known CD species as they were able to completely degrade all the three dyes and phenol in a short time scale. Moreover, exfoliated g-C_3N_4 was incorporated into the as-prepared G-CDs and it was found that the degradation rate constant for CD-C_3N_4 was further improved by 1.4 times, demonstrating an outstanding performance, which is attributed to a synergy between g-C_3N_4 and G-CDs. The radical trap experiments revealed that $O_2^{\cdot-}$ and holes were the dominant species generated within the G-CDs system, while for the CD-C_3N_4 system, $O_2^{\cdot-}$ and ·OH were the main active species. Furthermore, the excellent photocatalytic stability of G-CDs and CD-C_3N_4 were demonstrated with multiple cycles of dye degradation. Eventually, the cytotoxicity of G-CDs and CD-C_3N_4 were tested with a sea urchin *in vivo* model to exclude the risk of secondary pollution. These findings reveal insights into the development and design of CD species as a potential alternative for traditional heterogenous photocatalysts in remediation of hazardous contaminants in wastewater effluents. We anticipate that the use of G-CDs will open up new horizons for diverse photocatalytic applications.

CRediT authorship contribution statement

Yiqun Zhou: Conceptualization, Methodology, Validation, Formal analysis, Investigation, Writing - original draft, Writing - review & editing, Visualization, Supervision, Project administration. **Ahmed E. ElMetwally:** Conceptualization, Methodology, Val-

idation, Formal analysis, Investigation, Writing - original draft, Writing - review & editing, Visualization, Supervision, Project administration. **Jiuyan Chen:** Validation, Formal analysis, Investigation, Writing - review & editing. **Wenquan Shi:** Validation, Formal analysis, Investigation, Visualization. **Emel K. Cilingir:** Validation, Formal analysis, Investigation, Writing - review & editing, Visualization. **Brian Walters:** Formal analysis, Investigation, Visualization. **Keenan J. Mintz:** Validation, Formal analysis, Investigation, Writing - review & editing, Visualization. **Christian Martin:** Validation, Formal analysis, Investigation, Writing - review & editing, Visualization. **Braulio C.L.B. Ferreira:** Validation, Formal analysis, Investigation. **Wei Zhang:** Validation, Formal analysis, Investigation. **Sajini D. Hettiarachchi:** Writing - original draft. **Leonardo F. Serafim:** Writing - review & editing. **Patricia L. Blackwelder:** Validation, Formal analysis, Investigation, Writing - review & editing, Visualization. **Athula H. Wikramanayake:** Resources, Supervision. **Zhili Peng:** Resources, Writing - review & editing, Supervision, Funding acquisition. **Roger M. Leblanc:** Resources, Writing - review & editing, Supervision, Funding acquisition.

Declaration of Competing Interest

The authors declare that they have no known competing financial interests or personal relationships that could have appeared to influence the work reported in this paper.

Acknowledgements

Professor Roger M. Leblanc thanks the support from National Science Foundation under the grants 1809060 and 2041413. Also, authors gratefully acknowledge the great support from University of Miami, USA. Professor Zhili Peng acknowledges financial support from the National Natural Science Foundation of China under the grant 21807010, the Applied Basic Research Program of Yunnan Province (No. 2019FB066) and the "Double-First Class" University Construction Project (C176220200040) of Yunnan University.

Appendix A. Supplementary material

Supplementary data to this article can be found online at https://doi.org/10.1016/j.jcis.2021.04.121.

References

[1] R. MacDonald, Providing the world with clean water, Brit. Med. J. 327 (2003) 1416–1418.
[2] D. Perrone, S. Jasechko, Dry groundwater wells in the western United States, Environ. Res. Lett. 12 (2017) 104002–104012.
[3] B.R. Scanlon, C.C. Faunt, L. Longuevergne, R.C. Reedy, W.M. Alley, V.L. McGuire, P.B. McMahon, Groundwater depletion and sustainability of irrigation in the US High Plains and Central Valley, Proc. Natl. Acad. Sci. U. S. A. 109 (2012) 9320–9325.
[4] L.P. Galway, Boiling over: A descriptive analysis of drinking water advisories in first nations communities in Ontario, Canada, Int. J. Environ. Res. Public Health 13 (2016) 505–519.
[5] C.J. Talbot, E.M. Bennett, K. Cassell, D.M. Hanes, E.C. Minor, H. Paerl, P.A. Raymond, R. Vargas, P.G. Vidon, W. Wollheim, M.A. Xenopoulos, The impact of flooding on aquatic ecosystem services, Biogeochemistry 141 (2018) 439–461.
[6] M.R. Landsman, L.S. Rowles, S.H. Brodfuehrer, J.P. Maestre, K.A. Kinney, M.J. Kirisits, D.F. Lawler, L.E. Katz, Impacts of hurricane Harvey on drinking water quality in two Texas cities, Environ. Res. Lett. 14 (2019) 124046–124055.
[7] C. Peng, J.T. He, M.L. Wang, Z.G. Zhang, L. Wang, Identifying and assessing human activity impacts on groundwater quality through hydrogeochemical anomalies and NO_3^-, NH_4^+, and COD contamination: A case study of the Liujiang River Basin, Hebei Province, P.R. China, Environ. Sci. Pollut. Res. 25 (2018) 3539–3556.
[8] P.K. Amar, Ensuring safe water in post-chemical, biological, radiological and nuclear emergencies, J. Pharm. Bioallied. Sci. 2 (2010) 253–266.
[9] Z.-P. Zhong, N.E. Solonenko, Y.-F. Li, M.C. Gazitúa, S. Roux, M.E. Davis, J.L. Van Etten, E. Mosley-Thompson, V.I. Rich, M.B. Sullivan, L.G. Thompson, Glacier ice archives fifteen-thousand-year-old viruses, bioRxiv, 2020, doi: 10.1101/2020.01.03.894675.
[10] C. Wang, H. Liu, Y. Qu, TiO_2-based photocatalytic process for purification of polluted water: Bridging fundamentals to applications, J. Nanomater. 2013 (2013) 319637–319650.
[11] A. Bhati, S.R. Anand, Gunture, A.K. Garg, P. Khare, S.K. Sonkar, Sunlight-induced photocatalytic degradation of pollutant dye by highly fluorescent red-emitting Mg-N-embedded carbon dots, ACS Sustain. Chem. Eng. 6 (2018) 9246–9256.
[12] A.J. Englande Jr., P. Krenkel, J. Shamas, Wastewater treatment & water reclamation, Reference Module Earth Syst. Environ. Sci. (2015), https://doi.org/10.1016/B978-0-12-409548-9.09508-7.
[13] A.C. Mecha, M.N. Chollom, Photocatalytic ozonation of wastewater: A review, Environ. Chem. Lett. 18 (2020) 1491–1507.
[14] M. Abdennouri, M. Baâlala, A. Galadi, M. El Makhfouk, M. Bensitel, K. Nohair, M. Sadiq, A. Boussaoud, N. Barka, Photocatalytic degradation of pesticides by titanium dioxide and titanium pillared purified clays, Arab. J. Chem. 9 (2016) S313–S318.
[15] N. Daneshvar, D. Salari, A. Niaei, A.R. Khataee, Photocatalytic degradation of the herbicide Erioglaucine in the presence of nanosized titanium dioxide: Comparison and modeling of reaction kinetics, J. Environ. Sci. Health B 41 (2006) 1273–1290.
[16] R. Wang, X. Ma, T. Liu, Y. Li, L. Song, S.C. Tjong, L. Cao, W. Wang, Q. Yu, Z. Wang, Degradation aspects of endocrine disrupting chemicals: A review on photocatalytic processes and photocatalysts, Appl. Catal. A 597 (2020) 117547–117559.
[17] C.N. Paiva, M.T. Bozza, Are reactive oxygen species always detrimental to pathogens?, Antioxid. Redox Signal. 20 (2014) 1000–1037.
[18] A. Habibi-Yangjeh, S. Asadzadeh-Khaneghah, S. Feizpoor, A. Rouhi, Review on heterogeneous photocatalytic disinfection of waterborne, airborne, and foodborne viruses: Can we win against pathogenic viruses?, J. Colloid Interface Sci. 580 (2020) 503–514.
[19] M. Dryden, J. Cooke, R. Salib, R. Holding, S.L.F. Pender, J. Brooks, Hot topics in reactive oxygen therapy: Antimicrobial and immunological mechanisms, safety and clinical applications, J. Glob. Antimicrob. Resist. 8 (2017) 194–198.
[20] P. Radhika, Investigation into the growth phase dependent sensitivity of *Mycobacterium aurum* to chlorine and quantification of reactive oxygen species, Int. J. Sci. Technol. Res. 2 (2013) 32–39.
[21] A. Ayala, M.F. Muñoz, S. Argüelles, Lipid peroxidation: Production, metabolism, and signaling mechanisms of malondialdehyde and 4-hydroxy-2-nonenal, Oxid. Med. Cell. Longev. 2014 (2014) 360438–360469.
[22] J. Cadet, T. Douki, D. Gasparutto, J.L. Ravanat, Oxidative damage to DNA: Formation, measurement and biochemical features, Mutat. Res. 531 (2003) 5–23.
[23] F.D. Guerra, M.F. Attia, D.C. Whitehead, F. Alexis, Nanotechnology for environmental remediation: Materials and applications, Molecules 23 (2018) 1760–1782.
[24] M. Haro, R. Abargues, I. Herraiz-Cardona, J. Martínez-Pastor, S. Giménez, Plasmonic versus catalytic effect of gold nanoparticles on mesoporous TiO_2 electrodes for water splitting, Electrochim. Acta 144 (2014) 64–70.
[25] W.-H. Hung, T.-M. Chien, C.-M. Tseng, Enhanced photocatalytic water splitting by plasmonic TiO_2-Fe_2O_3 cocatalyst under visible light irradiation, J. Phys. Chem. C 118 (2014) 12676–12681.
[26] X. Chen, Z. Wu, D. Liu, Z. Gao, Preparation of ZnO photocatalyst for the efficient and rapid photocatalytic degradation of azo dyes, Nanoscale Res. Lett. 12 (2017) 143–152.
[27] T. Saison, N. Chemin, C. Chanéac, O. Durupthy, L. Mariey, F. Maugé, V. Brezová, J.-P. Jolivet, New insights into $BiVO_4$ properties as visible light photocatalyst, J. Phys. Chem. C 119 (2015) 12967–12977.
[28] L. Cheng, Q. Xiang, Y. Liao, H. Zhang, CdS-Based photocatalysts, Energy Environ. Sci. 11 (2018) 1362–1391.
[29] J. Wang, Y.-F. Lim, G. Wei Ho, Carbon-ensemble-manipulated ZnS heterostructures for enhanced photocatalytic H2 evolution, Nanoscale, 6 (2014) 9673-9680.
[30] Z. Li, X. Meng, Z. Zhang, Recent development on MoS_2-based photocatalysis: A review, J. Photochem. Photobiol. C 35 (2018) 39–55.
[31] K. Qi, S.-Y. Liu, A. Zada, Graphitic carbon nitride, a polymer photocatalyst, J. Taiwan Inst. Chem. Eng. 109 (2020) 111–123.
[32] M.A.M. Khan, W. Khan, M. Ahamed, A.N. Alhazaa, Microstructural properties and enhanced photocatalytic performance of Zn doped CeO(2) nanocrystals, Sci. Rep. 7 (2017) 12560–12570.
[33] J. Liu, H. Zhang, P. Chen, N. Cui, X. Gao, Ti-Si photocatalyst for producing hydrogen synthesized by shock wave, AIP Conf. Proc. 1426 (2012) 1403–1406.
[34] S. Qian, C. Wang, W. Liu, Y. Zhu, W. Yao, X. Lu, An enhanced CdS/TiO_2 photocatalyst with high stability and activity: Effect of mesoporous substrate and bifunctional linking molecule, J. Mater. Chem. 21 (2011) 4945–4952.
[35] S. Asadzadeh-Khaneghah, A. Habibi-Yangjeh, g-C_3N_4/carbon dot-based nanocomposites serve as efficacious photocatalysts for environmental purification and energy generation: A review, J. Clean. Prod. 276 (2020) 124319–124337.
[36] Y. Zhou, E.M. Zahran, B.A. Quiroga, J. Perez, K.J. Mintz, Z. Peng, P.Y. Liyanage, R. R. Pandey, C.C. Chusuei, R.M. Leblanc, Size-dependent photocatalytic activity of carbon dots with surface-state determined photoluminescence, Appl. Catal. B 248 (2019) 157–166.

[37] W.-J. Ong, L.-L. Tan, Y.H. Ng, S.-T. Yong, S.-P. Chai, Graphitic carbon nitride ($g-C_3N_4$)-based photocatalysts for artificial photosynthesis and environmental remediation: Are we a step closer to achieving sustainability?, Chem. Rev. 116 (2016) 7159–7329.
[38] A. Akhundi, A. Habibi-Yangjeh, M. Abitorabi, S. Rahim Pouran, Review on photocatalytic conversion of carbon dioxide to value-added compounds and renewable fuels by graphitic carbon nitride-based photocatalysts, Catal. Rev. 61 (2019) 595–628.
[39] A. Akhundi, A. Badiei, G.M. Ziarani, A. Habibi-Yangjeh, M.J. Muñoz-Batista, R. Luque, Graphitic carbon nitride-based photocatalysts: Toward efficient organic transformation for value-added chemicals production, Mol. Catal. 488 (2020) 110902–110915.
[40] M. Sachsenhauser, K. Walczak, P.A. Hampel, M. Stutzmann, I.D. Sharp, J.A. Garrido, Suppression of photoanodic surface oxidation of n-type 6H-SiC electrodes in aqueous electrolytes, Langmuir 32 (2016) 1637–1644.
[41] T. Jafari, E. Moharreri, A.S. Amin, R. Miao, W. Song, S.L. Suib, Photocatalytic water splitting-the untamed dream: A review of recent advances, Molecules 21 (2016) 900–928.
[42] A.M. Smith, S. Nie, Semiconductor nanocrystals: Structure, properties, and band gap engineering, Acc. Chem. Res. 43 (2010) 190–200.
[43] T. Vogler, P. Vöhringer, Probing the band gap of liquid ammonia with femtosecond multiphoton ionization spectroscopy, Phys. Chem. Chem. Phys. 20 (2018) 25657–25665.
[44] K.W. Böer, U.W. Pohl, The origin of band structure, Semiconductor Physics (2017) 1–20.
[45] L.K. Putri, W.-J. Ong, W.S. Chang, S.-P. Chai, Heteroatom doped graphene in photocatalysis: A review, Appl. Surf. Sci. 358 (2015) 2–14.
[46] J. Yu, C. Liu, K. Yuan, Z. Lu, Y. Cheng, L. Li, X. Zhang, P. Jin, F. Meng, H. Liu, Luminescence mechanism of carbon dots by tailoring functional groups for sensing Fe^{3+} ions, Nanomaterials (Basel) 8 (2018) 233–244.
[47] X. Wang, F. Wang, Y. Sang, H. Liu, Full-spectrum solar-light-activated photocatalysts for light-chemical energy conversion, Adv. Energy Mater. 7 (2017) 1700473–1700488.
[48] Y.-P. Sun, B. Zhou, Y. Lin, W. Wang, K.A.S. Fernando, P. Pathak, M.J. Meziani, B. A. Harruff, X. Wang, H. Wang, P.G. Luo, H. Yang, M.E. Kose, B. Chen, L.M. Veca, S.-Y. Xie, Quantum-sized carbon dots for bright and colorful photoluminescence, J. Am. Chem. Soc. 128 (2006) 7756–7757.
[49] Y. Wang, A. Hu, Carbon quantum dots: Synthesis, properties and applications, J. Mater. Chem. C 2 (2014) 6921–6939.
[50] Y. Zhou, K.J. Mintz, S.K. Sharma, R.M. Leblanc, Carbon dots: Diverse preparation, application, and perspective in surface chemistry, Langmuir 35 (2019) 9115–9132.
[51] Z. Peng, C. Ji, Y. Zhou, T. Zhao, R.M. Leblanc, Polyethylene glycol (PEG) derived carbon dots: Preparation and applications, Appl. Mater. Today 20 (2020) 100677–100692.
[52] Z. Peng, T. Zhao, Y. Zhou, S. Li, J. Li, R.M. Leblanc, Bone tissue engineering via carbon-based nanomaterials, Adv. Healthc. Mater. 9 (2020) 1901495–1901524.
[53] K.J. Mintz, Y. Zhou, R.M. Leblanc, Recent development of carbon quantum dots regarding their optical properties, photoluminescence mechanism, and core structure, Nanoscale 11 (2019) 4634–4652.
[54] K.J. Mintz, M. Bartoli, M. Rovere, Y. Zhou, S.D. Hettiarachchi, S. Paudyal, J. Chen, J.B. Domena, P.Y. Liyanage, R. Sampson, D. Khadka, R.R. Pandey, S. Huang, C.C. Chusuei, A. Tagliaferro, R.M. Leblanc, A deep investigation into the structure of carbon dots, Carbon 173 (2020) 433–447.
[55] Y. Li, J. Bi, S. Liu, H. Wang, C. Yu, D. Li, B.-W. Zhu, M. Tan, Presence and formation of fluorescence carbon dots in a grilled hamburger, Food Funct. 8 (2017) 2558–2565.
[56] S. Mandani, D. Dey, B. Sharma, T.K. Sarma, Natural occurrence of fluorescent carbon dots in honey, Carbon 119 (2017) 569–572.
[57] Z. Wang, H. Liao, H. Wu, B. Wang, H. Zhao, M. Tan, Fluorescent carbon dots from beer for breast cancer cell imaging and drug delivery, Anal. Methods 7 (2015) 8911–8917.
[58] T.V. de Medeiros, J. Manioudakis, F. Noun, J.-R. Macairan, F. Victoria, R. Naccache, Microwave-assisted synthesis of carbon dots and their applications, J. Mater. Chem. C 7 (2019) 7175–7195.
[59] C. Zheng, X. An, J. Gong, Novel pH sensitive N-doped carbon dots with both long fluorescence lifetime and high quantum yield, RSC Adv. 5 (2015) 32319–32322.
[60] D. Li, W. Li, H. Zhang, X. Zhang, J. Zhuang, Y. Liu, C. Hu, B. Lei, Far-red carbon dots as efficient light-harvesting agents for enhanced photosynthesis, ACS Appl. Mater. Interfaces 12 (2020) 21009–21019.
[61] R. Narayanan, M. Deepa, A.K. Srivastava, Förster resonance energy transfer and carbon dots enhance light harvesting in a solid-state quantum dot solar cell, J. Mater. Chem. A 1 (2013) 3907–3918.
[62] J. Hou, W. Wang, T. Zhou, B. Wang, H. Li, L. Ding, Synthesis and formation mechanistic investigation of nitrogen-doped carbon dots with high quantum yields and yellowish-green fluorescence, Nanoscale 8 (2016) 11185–11193.
[63] I. Srivastava, J.S. Khamo, S. Pandit, P. Fathi, X. Huang, A. Cao, R.T. Haasch, S. Nie, K. Zhang, D. Pan, Influence of electron acceptor and electron donor on the photophysical properties of carbon dots: A comparative investigation at the bulk-state and single-particle level, Adv. Funct. Mater. 29 (2019) 1902466–1902480.
[64] Z. Peng, Y. Zhou, C. Ji, J. Pardo, K.J. Mintz, R.R. Pandey, C.C. Chusuei, R.M. Graham, G. Yan, R.M. Leblanc, Facile synthesis of "boron-doped" carbon dots and their application in visible-light-driven photocatalytic degradation of organic dyes, Nanomaterials (Basel) 10 (2020) 1560–1576.
[65] H. Zhang, H. Ming, S. Lian, H. Huang, H. Li, L. Zhang, Y. Liu, Z. Kang, S.-T. Lee, Fe_2O_3/carbon quantum dots complex photocatalysts and their enhanced photocatalytic activity under visible light, Dalton Trans. 40 (2011) 10822–10825.
[66] H. Yu, Y. Zhao, C. Zhou, L. Shang, Y. Peng, Y. Cao, L.-Z. Wu, C.-H. Tung, T. Zhang, Carbon quantum dots/TiO_2 composites for efficient photocatalytic hydrogen evolution, J. Mater. Chem. A 2 (2014) 3344–3351.
[67] A. Habibi-Yangjeh, S. Feizpoor, D. Seifzadeh, S. Ghosh, Improving visible-light-induced photocatalytic ability of TiO_2 through coupling with Bi_3O_4Cl and carbon dot nanoparticles, Sep. Purif. Technol. 238 (2020) 116404–116417.
[68] S. Feizpoor, A. Habibi-Yangjeh, D. Seifzadeh, S. Ghosh, Combining carbon dots and $Ag_6Si_2O_7$ nanoparticles with TiO_2: Visible-light-driven photocatalysts with efficient performance for removal of pollutants, Sep. Purif. Technol. 248 (2020) 116928–116938.
[69] S. Muthulingam, K.B. Bae, R. Khan, I.-H. Lee, P. Uthirakumar, Carbon quantum dots decorated N-doped ZnO: Synthesis and enhanced photocatalytic activity on UV, visible and daylight sources with suppressed photocorrosion, J. Environ. Chem. Eng. 4 (2016) 1148–1155.
[70] Z. Cheng, F. Wang, T.A. Shifa, K. Liu, Y. Huang, Q. Liu, C. Jiang, J. He, Carbon dots decorated vertical SnS_2 nanosheets for efficient photocatalytic oxygen evolution, Appl. Phys. Lett. 109 (2016) 053905–053909.
[71] Y. Zhang, M. Park, H.Y. Kim, B. Ding, S.-J. Park, A facile ultrasonic-assisted fabrication of nitrogen-doped carbon dots/BiOBr up-conversion nanocomposites for visible light photocatalytic enhancements, Sci. Rep. 7 (2017) 45086–45097.
[72] S. Asadzadeh-Khaneghah, A. Habibi-Yangjeh, K. Nakata, Decoration of carbon dots over hydrogen peroxide treated graphitic carbon nitride: Exceptional photocatalytic performance in removal of different contaminants under visible light, J. Photochem. Photobiol. A 374 (2019) 161–172.
[73] Y. Zhou, A. Desserre, S.K. Sharma, S. Li, M.H. Marksberry, C.C. Chusuei, P.L. Blackwelder, R.M. Leblanc, Gel-like carbon dots: Characterization and their potential applications, ChemPhysChem 18 (2017) 890–897.
[74] Y. Zhou, K.J. Mintz, L. Cheng, J. Chen, B.C.L.B. Ferreira, S.D. Hettiarachchi, P.Y. Liyanage, E.S. Seven, N. Miloserdov, R.R. Pandey, B. Quiroga, P.L. Blackwelder, C.C. Chusuei, S. Li, Z. Peng, R.M. Leblanc, Direct conjugation of distinct carbon dots as Lego-like building blocks for the assembly of versatile drug nanocarriers, J. Colloid Interface Sci. 576 (2020) 412–425.
[75] A. Nickheslat, M.M. Amin, H. Izanloo, A. Fatehizadeh, S.M. Mousavi, Phenol photocatalytic degradation by advanced oxidation process under ultraviolet radiation using titanium dioxide, J. Environ. Public Health 2013 (2013) 815310–815319.
[76] Y. Li, X. Feng, Z. Lu, H. Yin, F. Liu, Q. Xiang, Enhanced photocatalytic H_2-production activity of C-dots modified $g-C_3N_4/TiO_2$ nanosheets composites, J. Colloid Interface Sci. 513 (2018) 866–876.
[77] H. Gao, J. Xu, J. Zhou, S. Zhang, R. Zhou, Metal organic framework derived heteroatoms and cyano (CN) group co-decorated porous $g-C_3N_4$ nanosheets for improved photocatalytic H_2 evolution and uranium(VI) reduction, J. Colloid Interface Sci. 570 (2020) 125–134.
[78] F. Li, H. Zhou, J. Fan, Q. Xiang, Amine-functionalized graphitic carbon nitride decorated with small-sized Au nanoparticles for photocatalytic CO_2 reduction, J. Colloid Interface Sci. 570 (2020) 11–19.
[79] J. Li, S. Ma, X. Xiao, D. Zhao, The one-step preparation of green-emissioned carbon dots through hydrothermal route and its application, J. Nanomater. 2019 (2019) 8628354–8628364.
[80] Y. Zhou, P.Y. Liyanage, D.L. Geleroff, Z. Peng, K.J. Mintz, S.D. Hettiarachchi, R.R. Pandey, C.C. Chusuei, P.L. Blackwelder, R.M. Leblanc, Photoluminescent carbon dots: A mixture of heterogeneous fractions, ChemPhysChem 19 (2018) 2589–2597.
[81] J. Xu, L. Zhang, R. Shi, Y. Zhu, Chemical exfoliation of graphitic carbon nitride for efficient heterogeneous photocatalysis, J. Mater. Chem. A 1 (2013) 14766–14772.
[82] D.W. Moore, J.A. Happe, The proton magnetic resonance spectra of some metal vinyl compounds, J. Phys. Chem. 65 (1961) 224–229.
[83] A. Pardo, D. Reyman, J.M.L. Poyato, F. Medina, Some β-carboline derivatives as fluorescence standards, J. Lumin. 51 (1992) 269–274.
[84] H. Kalita, J. Mohapatra, L. Pradhan, A. Mitra, D. Bahadur, M. Aslam, Efficient synthesis of rice based graphene quantum dots and their fluorescent properties, RSC Adv. 6 (2016) 23518–23524.
[85] X. Zhai, P. Zhang, C. Liu, T. Bai, W. Li, L. Dai, W. Liu, Highly luminescent carbon nanodots by microwave-assisted pyrolysis, ChemComm 48 (2012) 7955–7957.
[86] X.-F. Ding, L.-J. Wen, X. Zhou, Y.-Y. Ding, X.-C. Ye, L. Zhou, M.-C. Liu, H. Cai, J. Cao, Measurement of the fluorescence quantum yield of bis-MSB, Chin. Phys. C 39 (2015) 126001–126008.
[87] L. Segal, F.V. Eggerton, Infrared spectra of ethylenediamine and the dimethylethylenediamines, Appl. Spectrosc. 15 (1961) 116–117.
[88] S. Zhu, Q. Meng, L. Wang, J. Zhang, Y. Song, H. Jin, K. Zhang, H. Sun, H. Wang, B. Yang, Highly photoluminescent carbon dots for multicolor patterning, sensors, and bioimaging, Angew. Chem. Int. Ed. 52 (2013) 3953–3957.
[89] C.Y. Chang, A.A. Kashale, C.M. Lee, S.L. Chu, Y.F. Lin, I.W.P. Chen, Single atomically anchored iron on graphene quantum dots for a highly efficient oxygen evolution reaction, Mater. Today Energy 20 (2021) 100693–100701.

[90] A. Abdunazar, Y. Zhang, A. Muslim, L. Wang, H. Lan, Preparation and electrochemical characterization of carbon dots/polyaniline composite materials, Polym. Bull. 77 (2020) 1067–1080.
[91] T.C. Araújo, H.d.S. Oliveira, J.J.S. Teles, J.D. Fabris, L.C.A. Oliveira, J.P. de Mesquita, Hybrid heterostructures based on hematite and highly hydrophilic carbon dots with photocatalytic activity, Appl. Catal. B, 182 (2016) 204-212.
[92] N. Li, Z. Liu, M. Liu, C. Xue, Q. Chang, H. Wang, Y. Li, Z. Song, S. Hu, Facile synthesis of carbon dots@2D MoS_2 heterostructure with enhanced photocatalytic properties, Inorg. Chem. 58 (2019) 5746–5752.
[93] Z. Zhu, P. Yang, X. Li, M. Luo, W. Zhang, M. Chen, X. Zhou, Green preparation of palm powder-derived carbon dots co-doped with sulfur/chlorine and their application in visible-light photocatalysis, Spectrochim. Acta A 227 (2020) 117659–117665.
[94] Z. Ma, H. Ming, H. Huang, Y. Liu, Z. Kang, One-step ultrasonic synthesis of fluorescent N-doped carbon dots from glucose and their visible-light sensitive photocatalytic ability, New J. Chem. 36 (2012) 861–864.
[95] X. Yuan, C. Zhou, Y. Jin, Q. Jing, Y. Yang, X. Shen, Q. Tang, Y. Mu, A.-K. Du, Facile synthesis of 3D porous thermally exfoliated g-C_3N_4 nanosheet with enhanced photocatalytic degradation of organic dye, J. Colloid Interface Sci. 468 (2016) 211–219.
[96] L. Yuan, M.-Q. Yang, Y.-J. Xu, Tuning the surface charge of graphene for self-assembly synthesis of a $SnNb_2O_6$ nanosheet-graphene (2D–2D) nanocomposite with enhanced visible light photoactivity, Nanoscale 6 (2014) 6335–6345.
[97] H. Ji, F. Chang, X. Hu, W. Qin, J. Shen, Photocatalytic degradation of 2,4,6-trichlorophenol over g-C_3N_4 under visible light irradiation, Chem. Eng. J. 218 (2013) 183–190.
[98] F. Wang, Y. Feng, P. Chen, Y. Wang, Y. Su, Q. Zhang, Y. Zeng, Z. Xie, H. Liu, Y. Liu, W. Lv, G. Liu, Photocatalytic degradation of fluoroquinolone antibiotics using ordered mesoporous g-C_3N_4 under simulated sunlight irradiation: Kinetics, mechanism, and antibacterial activity elimination, Appl. Catal. B 227 (2018) 114–122.
[99] P.R. Sarika, P. Nancarrow, A. Khansaheb, T. Ibrahim, Bio-based alternatives to phenol and formaldehyde for the production of resins, Polymers 12 (2020) 2237–2260.
[100] A. Chen, G. Zhao, J. Chen, L. Chen, Y. Yu, Selective hydrogenation of phenol and derivatives over an ionic liquid-like copolymer stabilized palladium catalyst in aqueous media, RSC Adv. 3 (2013) 4171–4175.
[101] T.J. Parikh, Acute concentrated phenol dermal burns: Complications and management, Indian J. Crit. Care Med. 19 (2015) 280–282.